Biomaterials Science

PAPER

View Article Online
View Journal | View Issue

Cite this: *Biomater. Sci.*, 2019, **7**, 1973

Zein/gelatin/nanohydroxyapatite nanofibrous scaffolds are biocompatible and promote osteogenic differentiation of human periodontal ligament stem cells†

Qianmin Ou,‡[a] Yingling Miao, ‡[b] Fanqiao Yang,[c] Xuefeng Lin, [a] Li-Ming Zhang*[b] and Yan Wang *[a]

Received 19th December 2018,
Accepted 13th February 2019

DOI: 10.1039/c8bm01653d

rsc.li/biomaterials-science

In bone tissue engineering, it is important for biomaterials to promote the osteogenic differentiation of stem cells to achieve tissue regeneration. Therefore, it is critical to develop biomaterials with excellent cytocompatibility and osteoinductive ability. In our previous study, we found a zein/gelatin electrospinning scaffold with good biocompatibility, but low osteoinductive ability for human periodontal ligament stem cells (hPDLSCs). Therefore, herein, we fabricated novel zein/gelatin/nanohydroxyapatite (zein/gelatin/nHAp) nanofibrous membranes to overcome the drawbacks of the zein/gelatin scaffold. The results showed that the surface wettability of the zein/gelatin/nHAp nanofiber membranes was increased. Moreover, the inclusion of nHAp facilitated the attachment, proliferation, and osteogenic differentiation of hPDLSCs. Overall, the zein/gelatin/nHAp nanofiber membranes showed good biocompatibility and osteoinductive activity for hPDLSCs *in vitro* and *in vivo*; this suggested potential applications of these membranes in bone tissue engineering.

Introduction

Periodontitis is a chronic inflammatory disease that invades the gums and the supporting periodontal tissues, leading to an irreversible loss of attachment and alveolar bone resorption. It is difficult to restore the destroyed tissue in terms of structure and function once it is damaged. Conventional therapies currently applied to treat periodontal diseases have shown limited potential for complete periodontal regeneration.[1] The regeneration of a functional tooth-supporting attachment apparatus, especially osseous tissue, is of significant importance.[2,3] Human periodontal ligament stem cells (hPDLSCs) have characteristics similar to those of mesenchymal stem cells (MSCs) and are a type of stem cell discovered by Seo.[4] hPDLSCs have become a hotspot in periodontal tissue engineering because of their ease of access, low immunogenicity, multi-directional differentiation ability, and cementum-periodontal ligament complex formation.[5–8] However, only a few studies have been reported on biomaterials with osteoinductive abilities for hPDLSCs. Therefore, it is urgent to develop biomaterials that facilitate the cytocompatibility and osteogenic differentiation of hPDLSCs.

The extracellular matrix (ECM) is a complex interconnected structure composed of mucopolysaccharides and fibrin that provides mechanical strength and structural support for cells.[9] Electrospinning is a popular technique for generating fibres ranging from the nanometre to the micrometre scale to mimic the characteristics of the ECM to some extent.[9–11] Thus, electrospun nanofibers have been extensively applied in tissue engineering, wound repair, and drug delivery.[12,13] Zein and gelatin are natural polymers with excellent biocompatibility and biodegradability, which have been extensively investigated.[14–16] In our previous study, zein/gelatin membranes were fabricated by electrospinning, and their compatibility with hPDLSCs was evaluated.[17] The electrospun zein/gelatin membranes enhanced the attachment and growth of the hPDLSCs. However, hPDLSCs cultured on the electrospun zein/gelatin membranes showed weak alkaline phosphatase (ALP) activity. Therefore, it is necessary to incorporate a component with osteoinductive activity into the zein/gelatin nanofibres.

Hydroxyapatite (HAp) [$Ca_{10}(PO_4)_6(OH)_2$] is the main inorganic substitute of alveolar bone with high mechanical

[a]*Guanghua School of Stomatology, Sun Yat-sen University, Guangdong Provincial Key Laboratory of Stomatology, Guangzhou 510080, China. E-mail: wang93@mail.sysu.edu.cn; Tel: +86 2087330592*
[b]*School of Materials Science and Engineering, Sun Yat-sen University, Guangzhou 510275, China. E-mail: ceszhlm@mail.sysu.edu.cn; Tel: +86 2084112354*
[c]*Shunde hospital of Southern Medical University, Southern Medical University, Shunde, 528300, China*

†Electronic supplementary information (ESI) available. See DOI: 10.1039/c8bm01653d

‡The first two authors contributed equally to this study.

strength, good biocompatibility, and osteoinductive ability.[9,18,19] Natural crystalline hydroxyapatite in the needle form is about 15–200 nm in length, 10–80 nm in width, and 2–7 nm in thickness.[20] Therefore, compared to apatite, nano hydroxyapatite (nHAp) is more similar to natural bone in terms of crystallinity and morphology. The nHAp component is believed to promote the formation and deposition of calcium phosphate in the human body. It can enhance the intrinsic strength and biological activity of other biological materials and thus reduce their negative effects.[21–23] Thus, nHAp is considered to be the most promising material in bone regeneration.

In this study, we fabricated zein/gelatin/nHAp nanofiber membranes by electrospinning. The cytocompatibility of the zein/gelatin/nHAp membranes was evaluated by *in vitro* cell attachment and proliferation assays. The effects of the zein/gelatin/nHAp membranes on the osteogenic differentiation of hPDLSCs were investigated by *in vitro* and *in vivo* experiments (Scheme 1). The results of this study may provide useful information for scaffold selection in periodontal tissue regeneration.

Materials and methods

Materials

Alpha-minimum essential medium was purchased from Gibco (Grand Island, NY, USA). The osteogenic medium consisted of a standard culture medium supplemented with 100 μM L-ascorbic-2-phosphate, 20 μM dexamethasone, and 2 M β-glycerophosphate purchased from Sigma-Aldrich. Adipogenic medium was purchased from Cyagen Biosciences Inc. (Sunnyvale, CA, USA). The CellTiter 96 AQueous One Solution Cell Proliferation Assay (MTS) kit was obtained from Promega Corporation. Zein (Z3625), gelatin from porcine skin (gel strength = 300 g Bloom, Type A), and collagenase type I were purchased from Sigma. 1,1,1,3,3,3-Hexafluoro-2-propanol (HFIP, 99%) was purchased from Energy Chemical. Nano hydroxyapatite (nHAp, ≥97%, <100 nm particle size) was purchased from Aladdin.

Preparation of the nanofibrous membranes

Fabrication of the nanofibrous membranes. To fabricate zein/gelatin and zein/gelatin/nHAp scaffolds, 0.50 g of zein and 0.17 g of gelatin were dissolved in 5.0 mL of HFIP, and different amounts (0.05 g, 0.10 g, or 0.17 g) of nHAp were added to this solution, as presented in Table 1. During the electrospinning process, the homogeneously mixed solution was put in a syringe with a diameter of 5 mm, and the collector distance was 15 cm. The electrospun nanofibrous matrices of zein/gelatin, zein/gelatin/nHAp-1, zein/gelatin/nHAp-2, and zein/gelatin/nHAp-3 were prepared by applying a voltage of 20 kV and a solution flow rate of 0.6 mL h^{-1}. All these membranes were cut and placed in 48-well and 96-well plates. After the front and back of the membranes were subjected to UV irradiation for 2 h, the membranes were placed in tissue culture plates and washed three times with PBS. All samples were soaked in a standard medium for 12 hours before the cells were seeded for subsequent experiments.

Characterisation of the nanofibrous matrix. Surface morphologies of the electrospun zein/gelatin, zein/gelatin/nHAp-1, zein/gelatin/nHAp-2, and zein/gelatin/nHAp-3 fibre membranes were observed using scanning electron microscopy (SEM, JSM-6330F, Tokyo, Japan). The electrospun nanofibrous matrices were sputter-coated with gold and imaged by SEM at the accelerating voltage of 20 kV. The fibre diameters were analysed using an image analysis software (Image Plus 6). The

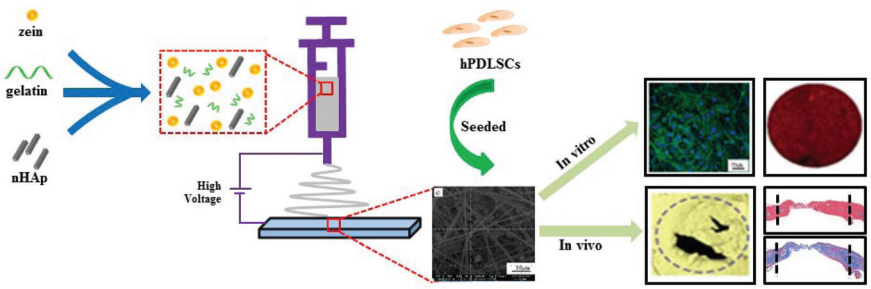

Scheme 1 The fabrication of electrospun membranes from zein, gelatin and nanohydroxyapatite (nHAp), and the effects of the membranes on the osteogenic differentiation of human periodontal ligament stem cells (hPDLSCs).

Table 1 Preparation conditions for the electrospun zein/gelatin/nHAp nanofibers with different compositions

Sample	Zein/gelatin (g/g)	nHAP (g)	HFIP (mL)	Zein ratio (w/w)	Gelatin ratio (w/w)	nHAp ratio (w/w)
Zein/gelatin	0.50/0.17	0	5.0	74.63%	25.37%	0
Zein/gelatin/nHAp-1	0.50/0.17	0.05	5.0	69.44%	23.61%	6.94%
Zein/gelatin/nHAp-2	0.50/0.17	0.10	5.0	64.94%	22.08%	12.98%
Zein/gelatin/nHAp-3	0.50/0.17	0.17	5.0	59.52%	20.24%	20.24%

average fibre diameter was determined by randomly selecting 300 fibres from each sample.

Characterisation of the contact angle of the nanofibrous matrix. The contact angles of the nanofibrous matrices were measured with deionised water using KRUSS DSA10-MK (KRUSS, Hamburg, Germany). Deionised water was automatically dropped onto the scaffold, and the contact angle was determined *via* triplicate measurements.

hPDLSC isolation and culture. Disease-free premolars were obtained from patients with orthodontic demands in the Affiliated Stomatological Hospital of Sun Yat-sen University. The research was approved by the ethics committee at the Affiliated Stomatological Hospital of Sun Yat-sen University (ERC-[2016]-46). Informed consents were obtained from the human participants in this study. The periodontal ligament tissues were scraped from the middle section of the root and enzymatically digested with 3 mg mL^{-1} collagenase type I and 4 mg mL^{-1} dispase for 1 hour. Subsequently, the tissues in the culture medium were placed on a tissue culture plate. After 8–10 days, the cells gradually migrated from the tissue blocks, and all the cells were obtained when they reached 80% confluence. The cells were then seeded at the density of 1200 cells per cm^2 on a culture plate. After 12 days, the cells were fixed with 4% paraformaldehyde and stained with 1% crystal violet. The colony-forming ability of the cells was observed by microscopy. A group of cells with higher than 50 cells was characterised as a colony, and images of single colonies were obtained by microscopy. The colony-forming cells were obtained, and cells at the passage 3–5 were used for subsequent experiments.

hPDLSC identification

Immunofluorescence staining. Cells were seeded at 2000 cells per cm^2 on a 24-well plate. After two days, the cells were fixed with 4% paraformaldehyde and permeabilized by 0.1% TritonX-100 at room temperature. Subsequently, the cells were incubated in 1% bovine serum albumin (BSA) for 30 min to block the non-specific binding sites. The cells were then incubated with primary antibodies against cytokeratin and vimentin (1 : 200, Abcam) for 1 hour followed by incubation with secondary antibodies (1 : 300, Abcam) for 45 min in the dark. After this, Hoechst 33342 (1 : 10 000; 1 mg mL^{-1}) was applied for nuclear staining. The results were observed, and images were obtained using fluorescence microscopy.

Flow cytometry. After collection, the cells were incubated with antibodies against CD34, CD44, CD45, CD90, CD105, and CD166 (FITC-labelled) for 1 h in the dark. After centrifugation at 800 rcf for 3 min, the cells were resuspended in 300 μL PBS. Fortessa flow cytometry was performed to detect the expression of the surface markers on the cells, and the results were analysed by the FlowJo software.

Osteogenic differentiation assay. For osteogenic differentiation, hPDLSCs were seeded at the density of 1×10^5 cells per cm^2 on a 24-well plate. After the cells reached 80% confluence, the medium was replaced by an osteogenic medium and changed every 2–3 days. After 28 days, the cells were fixed with 4% paraformaldehyde for 15 min at room temperature and stained with 2% Alizarin red (pH 4.2). After three times washing with PBS, calcium nodules were observed *via* a microscope and imaged.

Adipogenic differentiation assay. For adipogenic differentiation, hPDLSCs were seeded at the density of 1×10^5 cells per cm^2 on a 24-well plate. After the cells reached 100% confluence, the medium was replaced with the adipogenic medium, and the medium was changed every 2–3 days. After three weeks, the cells were fixed with 4% paraformaldehyde and stained with Oil red O at room temperature for 15 min. The lipid droplets were observed using a microscope, and images were obtained.

Biocompatibility and osteogenesis *in vitro* and *in vivo*

Cell adhesion and proliferation. Cell adhesion and proliferation were evaluated by an MTS assay. The hPDLSCs were seeded at the density of 8×10^3 cells per cm^2 on membranes in 96-well plates and cultured. Cell adhesion and proliferation were evaluated according to the manufacturer's instruction. After being rinsed with sterilized PBS, the cells were incubated with the MTS reagent for 3 hours at 37 °C under a 5% CO_2 atmosphere. The values of the optical density (OD) at 490 nm were determined for data analysis.

Cell morphology. The cell morphology was observed by F-actin staining using the Zeiss Axio Observer Z1 fluorescence microscope (Carl Zeiss, Oberkochen, Germany). The hPDLSCs were seeded at the density of 3500 cells per cm^2 on the membranes in 96-well plates. The cells were fixed with 4% paraformaldehyde, permeabilized by 0.1% Triton X-100, and blocked with 1% BSA for 30 min. The Actin-Tracker Green working agent was used to stain F-actin. After this, Hoechst 33342 was applied for nuclear staining, and the cells were washed three times with PBS. Cell spreading was observed, and images were obtained using a fluorescence microscope.

ALP activity. ALP activity was evaluated to investigate the osteogenic differentiation ability of the hPDLSCs cultured on membranes. The cells were seeded at the density of 6000 cells per cm^2 in 48-well plates, and the medium was changed every 2–3 days. Then, the cells were lysed, and the ALP activity was evaluated following the instructions of the ALP assay kit (Nanjing Jiancheng Bioengineering Institute, China). Absorbance was measured at the OD value of 520 nm.

Alizarin red staining. The hPDLSCs were seeded at 6000 cells per cm^2 on four different membranes in 48-well plates. After 14 days of culture, Alizarin red staining was applied to evaluate the formation of calcification nodules and performed as abovementioned. After all the images were obtained, calcium salt deposition in each group was determined using the hexadecyl pyridine semi-quantitative method. The OD values were obtained at 562 nm using a spectrophotometer for data analysis.

The real-time polymerase chain reaction. The levels of osteogenic differentiation-related genes (ALP, osteocalcin (OCN), and Runx2) in hPDLSCs cultured on scaffolds were assessed using the real-time polymerase chain reaction (RT-PCR). All

Table 2 Real-time polymerase chain reaction (RT-PCR) primers

Gene target	Sequence	Predicted size (bp)
ALP	Forward: 5′-GTGAACCGCAACTGGTACTC-3′ Reverse: 5′-GAGCTGCGTAGCGATGTCC-3′	81
OCN	Forward: 5′-CACTCCTCGCCCTATTGGC-3′ Reverse: 5′-CCCTCCTGCTTGGACACAAAG-3′	112
RUNX2	Forward: 5′-TGGTTACTGTCATGGCGGGTA-3′ Reverse: 5′-TCTCAGATCGTTGAACCTTGCTA-3′	101
GAPDH	Forward: 5′-AGCCACATCGCTCAGACAC-3′ Reverse: 5′-GCCCAATACGACCAAATCC-3′	67

primer sequences were designed according to Table 2. The hPDLSCs were seeded onto the zein/gelatin/nHAp membranes at 8000 cells per cm^2, and the cells were obtained. The total RNA was extracted by Trizol. The residual DNA was removed, and the total RNA extraction was followed by cDNA reverse-transcription. The PCR was performed using LightCycler 480 SYBR Green I Master, and the conditions were set as follows: initial denaturation at 95 °C for 10 min, 40 cycles of amplification at 95 °C for 15 s, 60 °C for 20 s, and 72 °C for 20 s. Data were analysed using the LightCycler 480 Software Version 1.5 and calculated using the comparative $2^{-\Delta\Delta Ct}$ method. GAPDH was set as the reference gene, and all the reactions were performed in triplicate.

Animal model. Herein, thirty male Sprague-Dawley rats (200–250 g) were used in the animal model. All animal procedures were performed in accordance with the Guidelines for Care and Use of Laboratory Animals of Sun Yat-Sen University and approved by the Institutional Animal Care and Use Committee of Sun Yat-Sen University (SYSU-IACUC-2018-000029). Under general anaesthesia, the cranium of the rats was exposed after medical incision. Then, two full-thickness bone defects of 5 mm diameter in symmetry were created by a dental machine. Both sides were implanted with the same type of membranes in three layers with/without hPDLSCs (2×10^6 cells). The groups were divided into (1) the zein/gelatin scaffold group, (2) the zein/gelatin/nHAp-1 scaffold group, (3) the zein/gelatin/nHAp-2 scaffold group, (4) the zein/gelatin/nHAp-2 + hPDLSCs group and (5) the zein/gelatin/nHAp-3 scaffold group. The incisions in all the animals were closed with surgical sutures in the fascia layer and skin layer. Postoperatively, all animals were kept in a warm area until they were awoken and allowed free activity in a cage. The animals were sacrificed after 6 and 12 weeks, and the whole calvarias were harvested. All specimens were washed three times with PBS and fixed in a 4% paraformaldehyde solution for 48 h at 4 °C.

Micro-computed tomography (CT) examination. A micro-CT scanner (SCANCO μCT50, Muttenz, Switzerland) was applied to detect the newly formed bone in the cranial defects of the rat animal model. A Mimics software (Mimics 17.0, Materialise, Leuven, Belgium) was applied to obtain three-dimensional images and calculate the bone mineral density of the new bone-like tissue.

Histological evaluation. After μCT scanning, the specimens (12 weeks) were subjected to histological evaluation. Briefly, the specimens were decalcified with a 10% EDTA solution (pH 7.4) for 1 month. Then, the samples were embedded for hematoxylin and eosin (HE) and masson trichrome (Masson) staining. All the samples were scanned by a tissue scanner equipment (Aperio, ScanScope XT, USA).

Statistical analysis

Statistical analyses were performed using the SPSS 20.0 software (SPSS, Chicago, IL, USA). Values are expressed as the mean ± SD. One-way-analysis of variance was used for comparison among the groups. $P < 0.05$ was considered as the statistical significance level, and $P < 0.01$ was considered as the higher significance level.

Results

Characterisation of the zein/gelatin/nHAp scaffolds

SEM of zein/gelatin/nHAp scaffold morphology. SEM images of the electrospun nanofibres are shown in Fig. 1. The morphology was not affected after the introduction of nHAp; however, the nHAp particles could be observed. All scaffolds presented highly porous networks, and the nHAp-containing groups had relatively rough surfaces. The incorporation of nHAp did not affect the obvious tensile strength of zein/gelatin nanofibers (Fig. S1 and Table S1†). The degradation rate of the zein/gelatin membranes was faster than that of the zein/gelatin/nHAp membranes (Fig. S2†). The increase in the concentration of nHAp caused the degradation rate to slow down in the zein/gelatin/nHAp-1, zein/gelatin/nHAp-2, and zein/gelatin/nHAp-3 membranes (Fig. S2†).

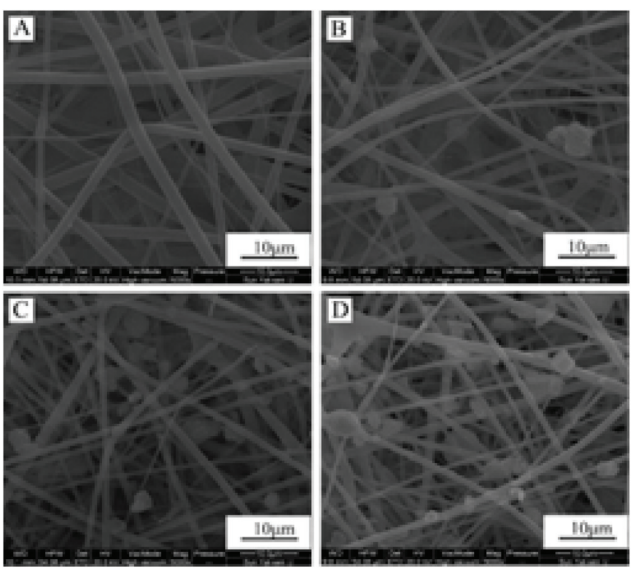

Fig. 1 SEM images of the electrospun zein/gelatin (A), zein/gelatin/nHAp-1 (B), zein/gelatin/nHAp-2 (C), and zein/gelatin/nHAp-3 (D) nanofibers.

Water contact angle measurement. The water contact angles of the zein/gelatin, zein/gelatin/nHAp-1, zein/gelatin/nHAp-2, and zein/gelatin/nHAp-3 nanofibrous matrices were 109.6 ± 1.6°, 84.1 ± 1.5°, 74.1 ± 1.3°, and 65.2 ± 0.9°, respectively. As the content of nHAp increased from 0 to 20%, the water contact angle decreased from 109.6° to 65.2° (Fig. 2). The results demonstrated that nHAp inclusion improved the surface wettability of the zein/gelatin membranes.

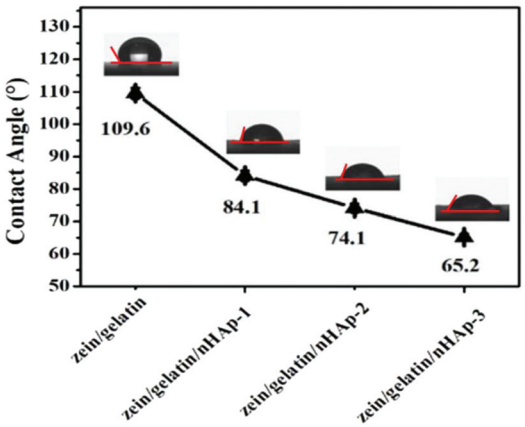

Fig. 2 Contact angles of the electrospun zein/gelatin, zein/gelatin/nHAp-1, zein/gelatin/nHAp-2, and zein/gelatin/nHAp-3 nanofibers.

Characterisation of the hPDLSCs. The primary cultured hPDLSCs gradually migrated from tissue blocks. Fig. 3A shows the formation of clonogenic clusters with plastic-adherent characteristics. Subsequently, the colony-forming cells were obtained and resuspended in a flask. The cells gradually extended from a spherical shape into the classic fusiform morphology displayed in Fig. 3B. The hPDLSCs positively expressed the MSC marker vimentin, but negatively expressed the epithelium marker cytokeratin (Fig. 3C and D, respectively); this indicated that the hPDLSCs were derived from the mesenchymal tissues. In terms of the multi-differentiation potential, the hPDLSCs exhibited Alizarin red-positive mineralised nodules and Oil Red O-positive lipid droplets after induction (Fig. 3E and F, respectively). Flow cytometry demonstrated that the hPDLSCs highly expressed the MSC surface markers CD44 (100%), CD90 (99.2%), CD105 (99.8%), and CD166

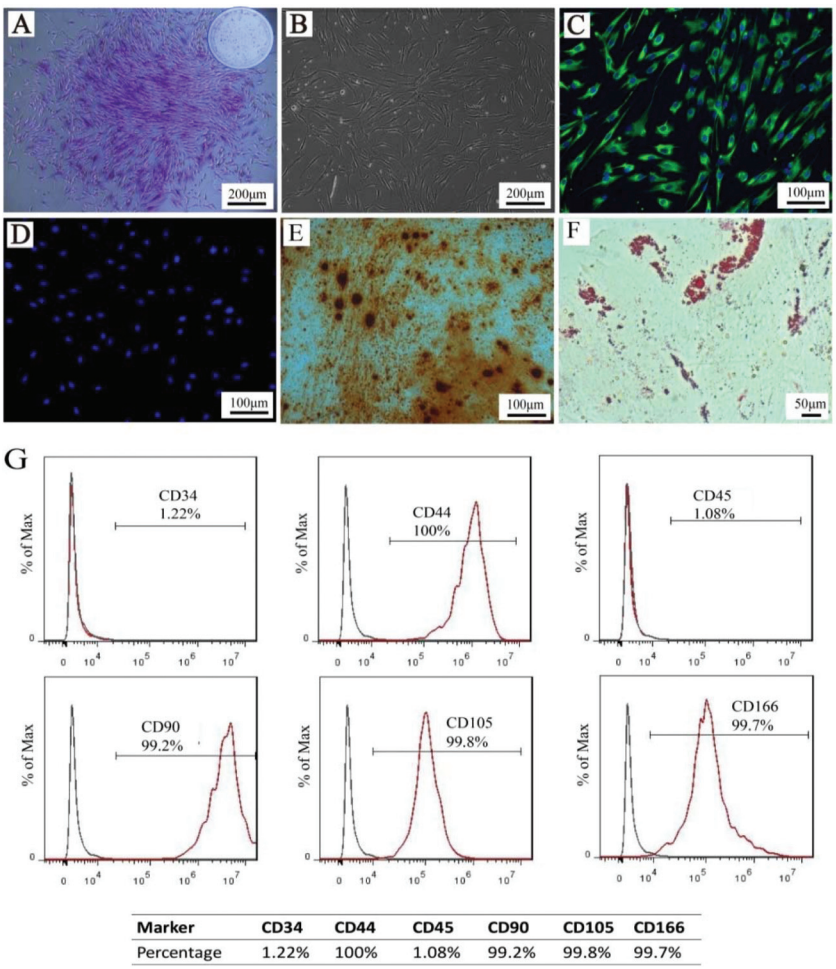

Marker	CD34	CD44	CD45	CD90	CD105	CD166
Percentage	1.22%	100%	1.08%	99.2%	99.8%	99.7%

Fig. 3 Characteristics of hPDLSCs. The morphology of a single-colony-forming unit of hPDLSCs (A). hPDLSCs adhered on a tissue culture plate in a spindle shape (B). hPDLSCs expressed vimentin (C), but not cytokeratin (D). Alizarin red staining (E) and Oil Red O staining (F) of the hPDLSCs. Surface markers of the hPDLSCs detected by flow cytometry (G).

(99.7%); on the other hand, low expression of the haematopoietic stem cell surface markers CD34 (1.22%) and CD45 (1.08%) was observed (Fig. 3G). Overall, the isolated hPDLSCs of mesenchymal origin were indeed successfully obtained.

Biocompatibility and osteogenesis *in vitro*

The cellular attachment and proliferation assay. The MTS assay was performed to evaluate the attachment and proliferation of hPDLSCs cultured on electrospun fibrous membranes at different times. The attachment of cells in the zein/gelatin/nHAp-2 group was significantly higher than that in the zein/gelatin group (Fig. 4A). Compared with the case of the zein/gelatin group, the proliferation of the hPDLSCs in the zein/gelatin/nHAp-2 group was significantly increased ($P < 0.01$, Fig. 4B). These results demonstrated that the zein/gelatin/nHAp-2 membrane was more beneficial for cell attachment and proliferation than the zein/gelatin membrane.

Cell morphology. The attachment and morphology of the hPDLSCs cultured on scaffolds were investigated by fluorescence staining. The cells tightly anchored on the surface of the scaffolds and exhibited an incompletely spread morphology on the first day (Fig. 5). This suggested that the cells were in the process of spreading. With a prolonged culture time, the cells continually stretched and eventually maintained a fully spread appearance. Furthermore, the number of attached cells on the nHAp-containing membranes was obviously higher than that on zein/gelatin (Fig. 5). The results indicated that zein/gelatin/nHAp facilitated the cell adhesion and growth.

Alizarin red staining. Alizarin red staining was applied to evaluate mineralisation in the hPDLSCs on the scaffolds. Fig. 6 shows that the positive staining of Alizarin red in terms of both area and density on the zein/gelatin/nHAp groups is higher than that on the zein/gelatin group. Zein/gelatin/nHAp-2 showed the highest amount of mineralised nodule formation. The results demonstrated that nHAp inclusion promoted the mineralisation of hPDLSCs.

ALP activity. The osteogenic differentiation of cells on the scaffolds was assessed by the ALP activity at 7 and 14 days. As shown in Fig. 7, the nHAp-containing membranes showed higher ALP expression than the zein/gelatin membrane; this indicated stronger osteogenic differentiation ability of the former membranes. Notably, the difference between the ALP activities of the zein/gelatin/nHAp-2 and zein/gelatin membranes was statistically significant ($p < 0.05$) at 7 and 14 days. The results suggested that the zein/gelatin/nHAp membranes provided a more beneficial environment for the osteogenic differentiation of hPDLSCs.

Real-time PCR analysis. To further determine the osteogenic differentiation of hPDLSCs on zein/gelatin/nHAp membranes, the osteogenesis-related genes were analysed. Fig. 7 presents the relative expression levels of ALP, OCN, and Runx2 of hPDLSCs on the scaffolds. After 7 and 14 days of culture, the gene expressions of ALP, OCN, and Runx2 were significantly elevated in the zein/gelatin/nHAp-2 and zein/gelatin/nHAp-3 groups as compared to those in the zein/gelatin group.

Biocompatibility and osteogenesis *in vivo*. Fig. 8 shows the formation of a new bone after the scaffolds were implanted for 6 and 12 weeks. The images showed that at 6 weeks, the defect area in the zein/gelatin scaffold was still large, and only a small amount of new bone was regenerated. However, the bone defect areas in the nHAp-containing scaffolds were smaller than those in the zein/gelatin scaffold. Moreover, the composite of hPDLSCs and zein/gelatin/nHAp-2 exhibited an obvious reduction in the bone defect area as compared to the zein/gelatin/nHAp-2 scaffold; this revealed that the environment provided by the zein/gelatin/nHAp membranes was conducive to the osteogenic differentiation of hPDLSCs. At 12 weeks, bone repair in the cranial defects was consistent with the trend observed at 6 weeks. Bone formation *in vivo* at 12 weeks was further analysed by histological staining. Similarly, the group of zein/gelatin/nHAp-2 seeded with hPDLSCs showed more new bone formation than the other scaffold groups (Fig. 9 and 10).

Discussion

Bioactive scaffolds are an indispensable element of bone tissue regeneration. Ideally, a biomaterial scaffold should best

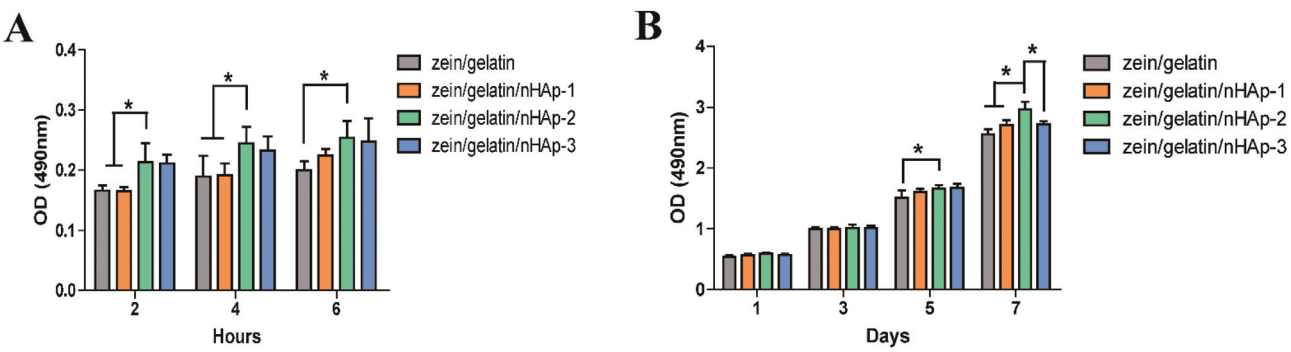

Fig. 4 Characterisation of cell attachment (A) and proliferation (B) on electrospun membranes containing zein/gelatin with different nHAp ratios at different times (*$P < 0.05$).

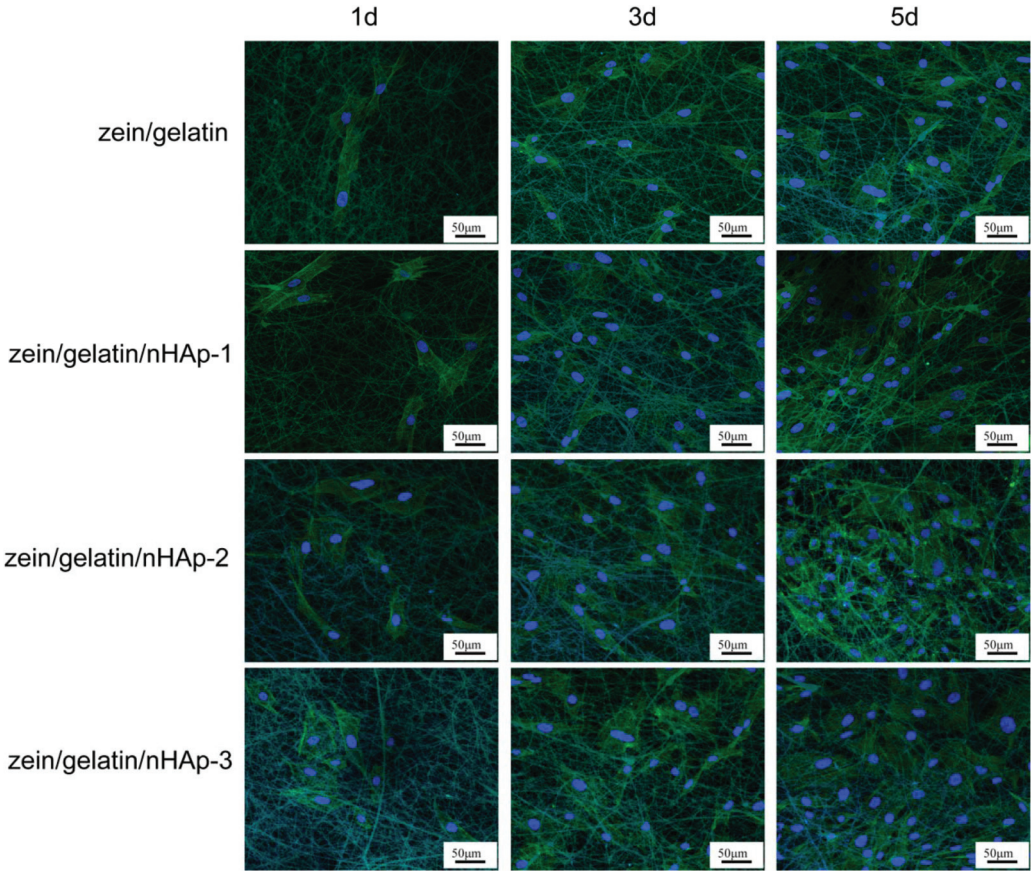

Fig. 5 F-Actin and nuclear staining of hPDLSCs on zein/gelatin, zein/gelatin/nHAp-1, zein/gelatin/nHAp-2, and zein/gelatin/nHAp-3 nanofibers on different days.

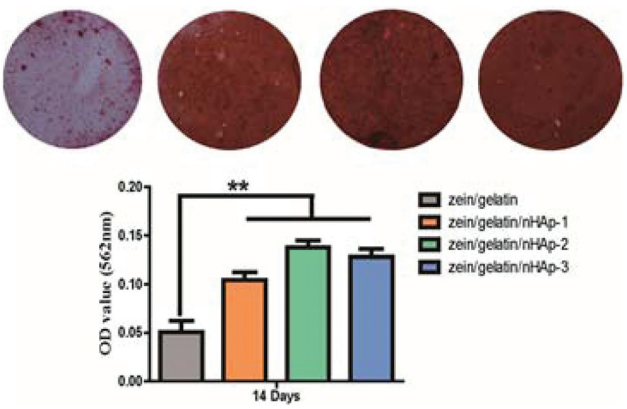

Fig. 6 The mineralisation ability of hPDLSCs cultured on zein/gelatin, zein/gelatin/nHAp-1, zein/gelatin/nHAp-2, and zein/gelatin/nHAp-3 nanofibers for 14 days. Semi-quantitative result of Alizarin red staining (**$P < 0.01$).

mimic the natural ECM in terms of compositional and structural features.[21,24] In this study, the electrospinning technique was applied to produce three-dimensional zein/gelatin/nHAp nanofibrous membranes with a porous interconnected nanostructure. The water contact angle of the membranes had a direct correlation with the mass ratio of nHAp, and the surface wettability was improved after the nHAp content was increased because of the hydrophilic nature of nHAp.[25] In a similar finding, it was reported the contact angle of poly (L-lactide) nanofibres was reduced by nHAp inclusion.[26]

The biocompatibility of biomaterials is one of the prerequisites for medical therapy and is closely related to the biological behaviour of cells when they are in contact with the biomaterials. The first interaction is cell attachment, followed by the natural process of cell spreading. Thus, the quality of the initial cell adhesion will affect the proliferation capacity as well as the directional differentiation of cells.[27–29] The attachment of the cells on the scaffolds increases the survival time and viability of the cells; the zein/gelatin/nHAp membranes in this study enable better cell adhesion in the early stages and better cell proliferation when compared with the zein/gelatin membranes because of multiple factors. First, the gelatin and nHAp components enhanced the surface wettability of the membrane, providing a hydrophilic microenvironment to promote cell affinity. Second, gelatin with short RGD oligopeptide sequences provided various integrin binding sites for cells.[30] Moreover, nHAp could adsorb adhesion proteins, such as fibronectin and vitronectin, on its surface; this led to a better binding of integrins to nHAp.[31] Third, the rough surface

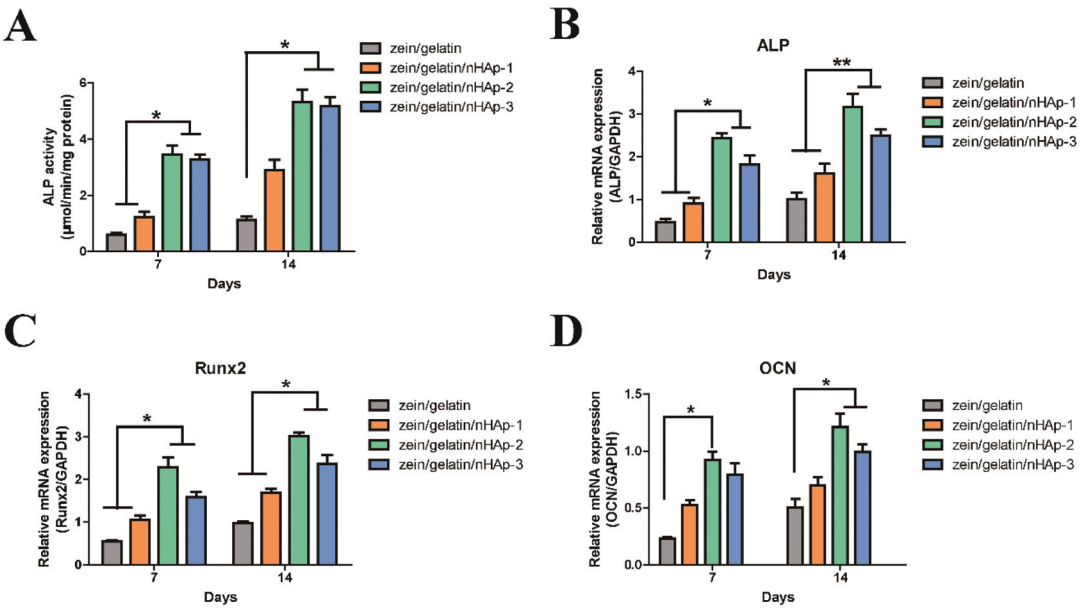

Fig. 7 ALP activity in human hPDLSCs cultured on different nanofiber membranes for 7 and 14 days (A). The expression of osteogenesis-related genes (ALP, OCN, and Runx2) in hPDLSCs cultured on different nanofibers membranes for 7 and 14 days (B–D; *$P < 0.05$, **$P < 0.01$).

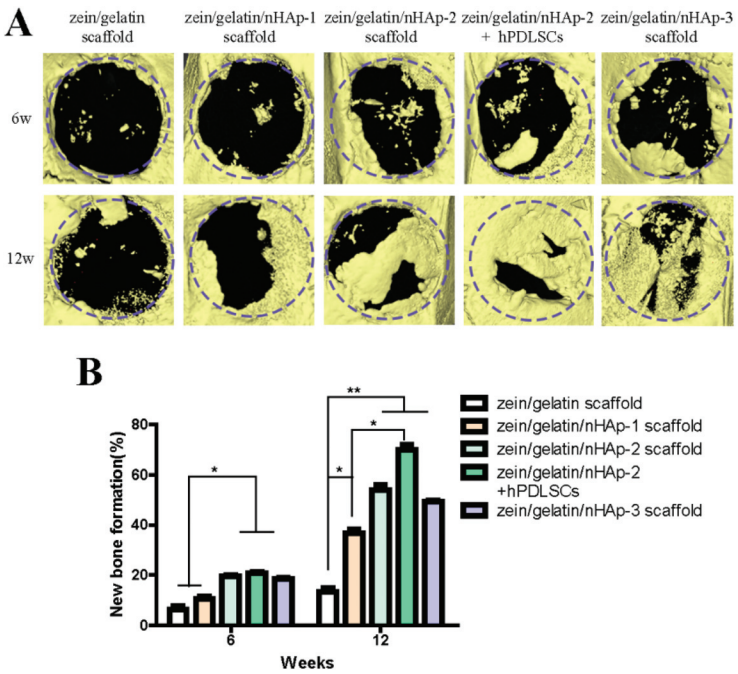

Fig. 8 Micro-CT images of new bone formation on the electrospun zein/gelatin, zein/gelatin/nHAp-1, zein/gelatin/nHAp-2, and zein/gelatin/nHAp-3 nanofibers at 6 and 12 weeks (A). New bone formation after the membranes were implanted (B; *$P < 0.05$, **$P < 0.01$).

of zein/gelatin/nHAp also favoured cell attachment.[32] Therefore, it takes a very short time for the hPDLSCs to adapt to the zein/gelatin/nHAp membranes.

Pore size is connected with the attachment, proliferation and infiltration of cells in tissue scaffolds.[33–35] The optimal pore size approximates the diameter of cells.[33] A small pore size limits the infiltration and ingrowth of cells into the nanofibers, whereas a large pore size prevents cell attachment due to an insufficient surface area.[36,37] Nowadays, there are many novel techniques for optimizing the pore size to improve the effectiveness of biomaterials such as the sacrificial fibres and the 3D gradient pore scaffolds.[36,38] The sacrificial fibres

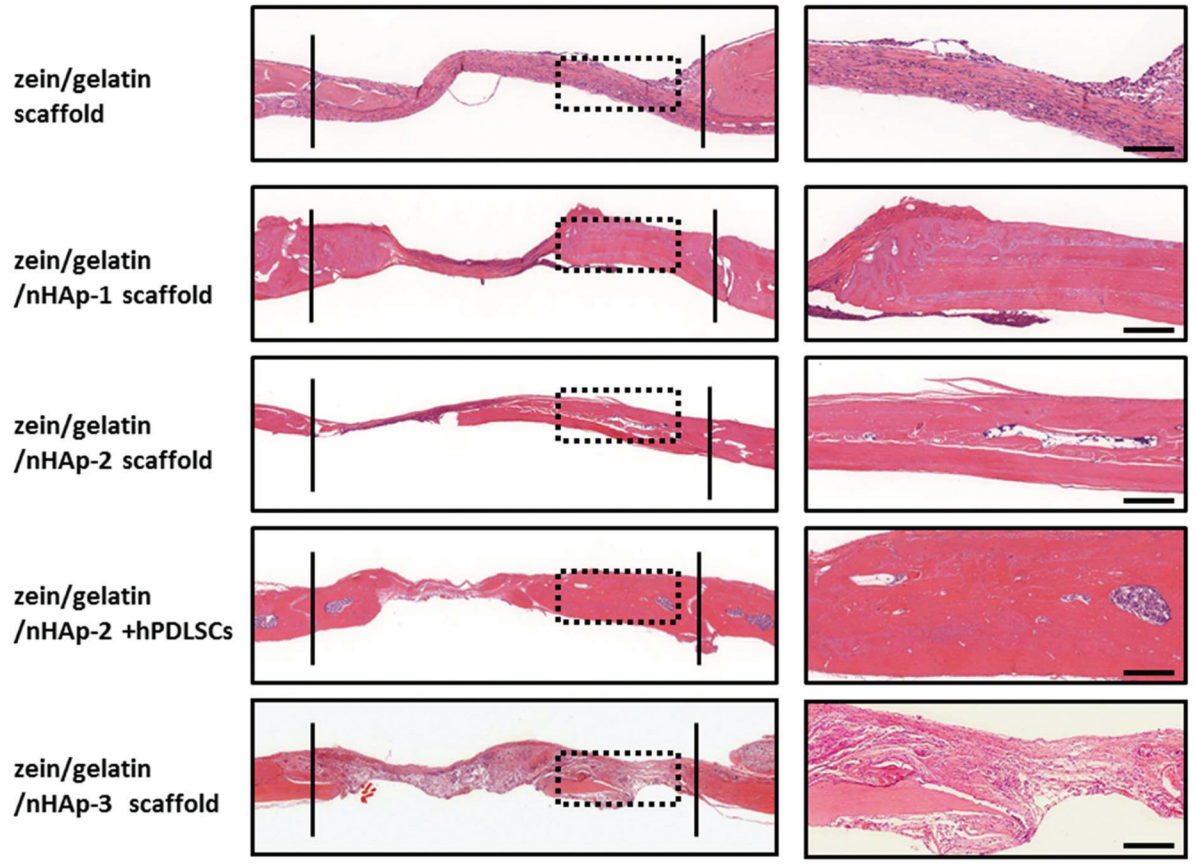

Fig. 9 HE staining for the bone formation at 12 weeks. Between the two solid lines is the newly formed bone. The images on the right are the high magnification images of the dotted box (bar: 500 m).

support infiltration, colonization and maturation of MC3T3-E1 pre-osteoblasts.[39] The 3D gradient pore scaffolds are beneficial for cell infiltration depth, which are promising biomaterials for tissue engineering with gradient pore sizes.[36] Therefore, we will focus on optimizing the pore size of the zein/gelatin/nHAp membranes in future research.

The osteoinductive bioactivity of a scaffold is essential for bone defect construction. In the zein/gelatin/nHAp nanofiber membranes, osteogenic biomarker genes (including ALP, OCN, and Runx2) were highly expressed. The results indicated that the addition of nHAp could effectively promote the differentiation of hPDLSCs towards the osteoblastic lineage. Calcium ions released from the partial dissolution of nHAp can promote osteogenic differentiation and bone mineralisation.[40] Moreover, nHAp could "cross-link" the fibres by mechanical interlocking or forming calcium ion bridges, thus having an osteoinductive function.[41] ALP is a widely recognised marker of early osteoblastic differentiation associated with undifferentiated pluripotent stem cells.[42,43] Runx2 is the key transcription factor that initiates and regulates early osteogenesis and late mineralisation of bone.[44,45] The high expression of ALP and Runx2 at 7 and 14 days illustrated that the zein/gelatin/nHAp membranes had positive effects on the differentiation of hPDLSCs into osteoblasts at the early stage. OCN, a non-collagenous protein exclusively synthesised by osteoblasts in the process of bone matrix mineralisation, is an important marker reflecting osteogenic activity in the late stage of maturation.[45,46] In addition, OCN is considered effective in controlling the nucleation of Hap crystals.[47]

During the process of stem cell differentiation into osteoblasts, osteoblast precursor cells could bind to nHAp *via* surface adhesion proteins.[31] Rat bone marrow stem cells cultured on silk fibroin fibres with 20 wt% HAp showed the best osteogenic differentiation ability.[48] However, polycaprolactone/HAp scaffolds with 15 wt% HAp content exhibited higher ALP activity.[49] In our study, the zein/gelatin/nHAp scaffolds with 13% nHAp facilitated robust osteogenesis. We speculate that the different results may be influenced by the cell phenotype, nHAp content, and constituents of the biomaterials and are worthy of further investigation.

To assess the ability of zein/gelatin/nHAp as scaffolds for hPDLSCs to promote bone repair *in vivo*, a rat cranial defect model was established. Micro-CT, HE staining and Masson staining showed new bone formation in the zein/gelatin/nHAp scaffolds and the composites of hPDLSCs and zein/gelatin/nHAp. These findings illustrated that both zein/gelatin/nHAp and hPDLSCs contributed to bone

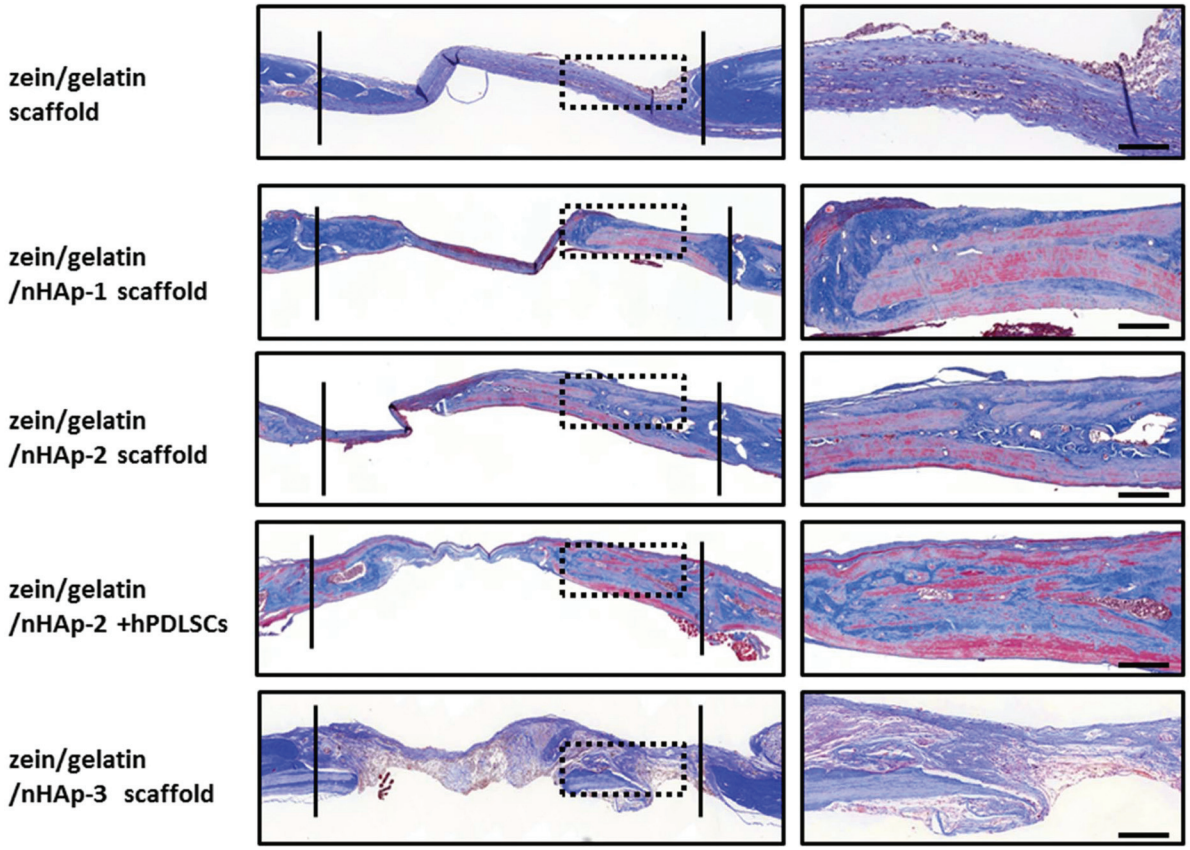

Fig. 10 Masson staining for the bone formation at 12 weeks. Between the two solid lines is the newly formed bone. The pictures on the right are the high magnification images of the dotted box (bar: 500 μm).

regeneration *in vivo*. Zein/gelatin/nHAp facilitated osteogenesis *in vivo* likely owing to the topography and components that mimic the ECM as well as the osteoinductive function of nHAp. The hPDLSCs may directly differentiate into osteocytes by secreting diverse soluble molecules to modulate the microenvironment because they have similar characteristics as MSCs.[50,51] Thus, further investigation is necessary to clarify the mechanism of zein/gelatin/nHAp in affecting the hPDLSC osteogenesis.

Conclusions

This study demonstrated that the electrospun zein/gelatin/nHAp nanofibres could facilitate the attachment, proliferation, and osteogenic differentiation of hPDLSCs. Moreover, the electrospun zein/gelatin/nHAp nanofibers had good biocompatibility and osteogenic activity *in vivo*. Hence, the electrospun zein/gelatin/nHAp membranes are a good candidate for applications in human bone tissue engineering.

Conflicts of interest

There are no conflicts to declare.

Acknowledgements

The authors acknowledge the funding support received from the Special Funds for Public Welfare Research and Capacity Building of Guangdong Province in China (No. 2014A010105025), the Natural Science Foundation of China (No. 81371793, 81530069) and the Guangdong Innovative Research Team program (No. 2009010058).

References

1 R. Pokrowiecki, K. Palka and A. Mielczarek, *Nanomedicine*, 2018, **13**, 639–667.
2 J. Han, D. Menicanin, S. Gronthos and P. M. Bartold, *Aust. Dent. J.*, 2014, **59**, 117–130.
3 F. Chen, H. Sun, H. Lu and Q. Yu, *Biomaterials*, 2012, **33**, 6320–6344.
4 B. M. Seo, M. Miura, S. Gronthos, P. M. Bartold, S. Batouli, J. Brahim, M. Young, P. G. Robey, C. Y. Wang and S. Shi, *Lancet*, 2004, **364**, 149–155.
5 W. Zhu and M. Liang, *Stem Cells Int.*, 2015, **2015**, 1–11.
6 M. Lei, K. Li, B. Li, L. N. Gao, F. M. Chen and Y. Jin, *Biomaterials*, 2014, **35**, 6332–6343.

7 C. Zhang, B. Yan, Z. Cui, S. Cui, T. Zhang, X. Wang, D. Liu, R. Yang, N. Jiang, Y. Zhou and Y. Liu, *Sci. Rep.*, 2017, **7**, 10519.
8 F. M. Chen, L. N. Gao, B. M. Tian, X. Y. Zhang, Y. J. Zhang, G. Y. Dong, H. Lu, Q. Chu, J. Xu, Y. Yu, R. X. Wu, Y. Yin, S. Shi and Y. Jin, *Stem Cell Res. Ther.*, 2016, **7**, 33.
9 J. Zhang, H. Liu, J. Ding, J. Wu, X. Zhuang, X. Chen, J. Wang, J. Yin and Z. Li, *ACS Biomater. Sci. Eng.*, 2016, **2**, 1471–1482.
10 C. Zhijiang, Z. Qin, S. Xianyou and L. Yuanpei, *Mater. Sci. Eng., C*, 2017, **71**, 797–806.
11 P. Pal, P. Dadhich, P. K. Srivas, B. Das, D. Maulik and S. Dhara, *Biomater. Sci.*, 2017, **5**, 1786–1799.
12 A. Deng, Y. Yang, S. Du and S. Yang, *Biomater. Sci.*, 2018, **6**, 2197–2208.
13 R. Pugliese, M. Maleki, R. N. Zuckermann and F. Gelain, *Biomater. Sci.*, 2018, **7**, 76–91.
14 J. Lin, J. Ding, Y. Dai, X. Wang, J. Wei and Y. Chen, *Mater. Sci. Eng., C*, 2017, **81**, 321–326.
15 S. Babitha, M. Annamalai, M. M. Dykas, S. Saha, K. Poddar, J. R. Venugopal, S. Ramakrishna, T. Venkatesan and P. S. Korrapati, *J. Tissue Eng. Regener. Med.*, 2018, **12**, 991–1001.
16 C. Sanhueza, F. Acevedo, S. Rocha, P. Villegas, M. Seeger and R. Navia, *Int. J. Biol. Macromol.*, 2018, **124**, 102–110.
17 F. Yang, Y. Miao, Y. Wang, L. Zhang and X. Lin, *Materials*, 2017, **10**, 1168.
18 A. Tampieri, A. Ruffini, A. Ballardini, M. Montesi, S. Panseri, F. Salamanna, M. Fini and S. Sprio, *Biomater. Sci.*, 2018, **7**, 307–321.
19 B. Li, P. Gao, H. Zhang, Z. Guo, Y. Zheng and Y. Han, *Biomater. Sci.*, 2018, **6**, 3202–3218.
20 A. El-Fiqi, J. O. Buitrago, S. H. Yang and H. W. Kim, *Acta Biomater.*, 2017, **60**, 38–49.
21 G. Dalmonico, P. F. Franczak, N. J. Levandowski, N. Camargo, A. L. Dallabrida, C. B. Da, O. G. Gil, O. Cambra-Moo, M. A. Rodriguez and M. Canillas, *Biomater. Sci.*, 2017, **5**, 1315–1325.
22 M. Ribeiro, M. P. Ferraz, F. J. Monteiro, M. H. Fernandes, M. M. Beppu, D. Mantione and H. Sardon, *Nanomedicine*, 2017, **13**, 231–239.
23 X. Wang, X. Wu, H. Xing, G. Zhang, Q. Shi, L. E, N. Liu, T. Yang, D. Wang, F. Qi, L. Wang and H. Liu, *ACS Appl. Mater. Interfaces*, 2017, **9**, 11380–11391.
24 S. Wang, F. Hu, J. Li, S. Zhang, M. Shen, M. Huang and X. Shi, *Nanomedicine*, 2018, **14**, 2505–2520.
25 H. Samadian, M. Salehi, S. Farzamfar, A. Vaez, A. Ehterami, H. Sahrapeyma, A. Goodarzi and S. Ghorbani, *Artif. Cells, Nanomed., Biotechnol.*, 2018, 1–11.
26 S. Fu, P. Ni, B. Wang, B. Chu, J. Peng, L. Zheng, X. Zhao, F. Luo, Y. Wei and Z. Qian, *Biomaterials*, 2012, **33**, 8363–8371.
27 M. I. Hassan and N. Sultana, *3 Biotech.*, 2017, **7**, 249.
28 J. E. Song, N. Tripathy, D. H. Lee, J. H. Park and G. Khang, *ACS Appl. Mater. Interfaces*, 2018, **10**, 32955–32964.
29 J. Wu, K. Zhang, X. Yu, J. Ding, L. Cui and J. Yin, *Biomater. Sci.*, 2017, **5**, 2251–2267.
30 A. R. El-Ghannam, P. Ducheyne, M. Risbud, C. S. Adams, I. M. Shapiro, D. Castner, S. Golledge and R. J. Composto, *J. Biomed. Mater. Res., Part A*, 2004, **68**, 615–627.
31 H. Liu, H. Peng, Y. Wu, C. Zhang, Y. Cai, G. Xu, Q. Li, X. Chen, J. Ji, Y. Zhang and H. W. OuYang, *Biomaterials*, 2013, **34**, 4404–4417.
32 H. J. Wang, M. Q. Li, W. Liu, G. D. Yao, M. Y. Xia, T. Hayashi, H. Fujisaki, S. Hattori, S. Tashiro, S. Onodera and T. Ikejima, *Connect. Tissue Res.*, 2016, **57**, 262–269.
33 A. Paim, I. C. Tessaro, N. Cardozo and P. Pranke, *J. Biol. Phys.*, 2018, **44**, 245–271.
34 J. Zhang, T. Zheng, E. Alarcin, B. Byambaa, X. Guan, J. Ding, Y. S. Zhang and Z. Li, *Small*, 2017, **13**, 1949.
35 Z. Z. Zhang, D. Jiang, J. X. Ding, S. J. Wang, L. Zhang, J. Y. Zhang, Y. S. Qi, X. S. Chen and J. K. Yu, *Acta Biomater.*, 2016, **43**, 314–326.
36 L. Huang, J. Huang, H. Shao, X. Hu, C. Cao, S. Fan, L. Song and Y. Zhang, *Mater. Sci. Eng., C*, 2019, **94**, 179–189.
37 J. Li, W. Xu, D. Li, T. Liu, Y. S. Zhang, J. Ding and X. Chen, *ACS Nano*, 2018, **12**, 6685–6699.
38 J. Wu and Y. Hong, *Bioact. Mater.*, 2016, **1**, 56–64.
39 B. M. Whited, J. R. Whitney, M. C. Hofmann, Y. Xu and M. N. Rylander, *Biomaterials*, 2011, **32**, 2294–2304.
40 X. Wu, L. Miao, Y. Yao, W. Wu, Y. Liu, X. Chen and W. Sun, *Int. J. Nanomed.*, 2014, **9**, 4135–4143.
41 C. Hellmich and F. J. Ulm, *J. Biomech.*, 2002, **35**, 1199–1212.
42 P. M. Favi, R. S. Benson, N. R. Neilsen, R. L. Hammonds, C. C. Bates, C. P. Stephens and M. S. Dhar, *Mater. Sci. Eng., C*, 2013, **33**, 1935–1944.
43 J. Tan, D. Wang, H. Cao, Y. Qiao, H. Zhu and X. Liu, *ACS Appl. Mater. Interfaces*, 2018, **10**, 15724.
44 T. Wang, X. Yang, X. Qi and C. Jiang, *J. Transl. Med.*, 2015, **13**, 152.
45 S. K. Boda, G. Thrivikraman, B. Panigrahy, D. D. Sarma and B. Basu, *ACS Appl. Mater. Interfaces*, 2017, **9**, 19389–19408.
46 X. Chen, S. Bai, B. Li, H. Liu, G. Wu, S. Liu and Y. Zhao, *Int. J. Nanomed.*, 2016, **11**, 4707–4718.
47 M. Sila-Asna, A. Bunyaratvej, S. Maeda, H. Kitaguchi and N. Bunyaratavej, *Kobe J. Med. Sci.*, 2007, **53**, 25–35.
48 B. Niu, B. Li, Y. Gu, X. Shen, Y. Liu and L. Chen, *J. Biomater. Sci., Polym. Ed.*, 2017, **28**, 257–270.
49 S. Eosoly, N. E. Vrana, S. Lohfeld, M. Hindie and L. Looney, *Mater. Sci. Eng., C*, 2012, **32**, 2250–2257.
50 Y. Fu, S. Liu, S. J. Cui, X. X. Kou, X. D. Wang, X. M. Liu, Y. Sun, G. N. Wang, Y. Liu and Y. H. Zhou, *ACS Appl. Mater. Interfaces*, 2016, **8**, 15958–15966.
51 L. Li, W. Liu, H. Wang, Q. Yang, L. Zhang, F. Jin and Y. Jin, *Cell Death Dis.*, 2018, **9**, 480.